Title
A Reliable Direct Drive for the Steering Wheel Column of Buses

Authors
Eirea, Gabriel
Sanders, Seth
Zhang, Wei-Bin

Publication Date
2005-11-01

CALIFORNIA PATH PROGRAM
INSTITUTE OF TRANSPORTATION STUDIES
UNIVERSITY OF CALIFORNIA, BERKELEY

A Reliable Direct Drive for the Steering Wheel Column of Buses

Gabriel Eirea
Seth Sanders
Wei-Bin Zhang

California PATH Research Report
UCB-ITS-PRR-2005-37

This work was performed as part of the California PATH Program of the University of California, in cooperation with the State of California Business, Transportation, and Housing Agency, Department of Transportation, and the United States Department of Transportation, Federal Highway Administration.

Final Report for RTA 64A0028

November 2005

ISSN 1055-1425

A Reliable Direct Drive for the Steering Wheel Column of Buses

Part 2 report for Development of Precision Docking Function for Bus Rapid Transit

Gabriel Eirea, Seth Sanders and Wei-Bin Zhang

1. Introduction

BRT has demonstrated its effectiveness to be a portion of the 'backbone' of an integrated transit network. It has become an effective means for attracting non-traditional transit riders and therefore can help to reduce urban transportation needs and traffic congestion. Many California transit agencies are planning to deploy BRT and have considered the use of dedicated lanes for BRT to be a very attractive option as it is less affected by automobile traffic and therefore can provide rail-like quality of service. In 1999, Caltrans generated a Caltrans Action Request (CAR) to request participation in the Bus Rapid Transit Project with VTA and other local transit providers. The future of BRT in California, as envisioned by Caltrans, would include a system of coordinated transit infrastructure, equipment, and operations that will give preference to buses on local urban transportation systems and the High Occupancy Vehicles (HOVs) lanes at congested corridors. The goal of the BRT service is to attract riders from single-occupancy vehicles, which could result in congestion relief without major infrastructure expansion. In the long-term, the proposed project may integrate the currently separate local transportation systems and transit services (offered by multiple transit agencies in a region) to provide express transit services enabled by interconnectivity between local systems and the State highway HOV system. Under the Caltrans Action Request, a BRT research program is established. One of the elements of this program is **"**Development of Precision Docking Function for Bus Rapid transit (named 'Precision Docking' or BPD from hereon)".

Precision docking -- an innovative technology that enable bus to perform rail like level boarding has shown great potential for allowing fast boarding and alighting and therefore reducing the total trip time and improving service reliability and quality for BRT system. The bus precision docking seeks to achieve, with the help of electronic guidance technologies, a high docking accuracy and consistency that allows fast loading and unloading of passengers with special needs. In addition to the potential of serving as a major component of an advanced bus stop, such an automation capability would also reduce the skill and training requirements on the bus driver as well as the stress associated with achieving the high accuracy by the driver. In addition to precision docking, electronic guidance technologies also support a number of critical functions for BRT and transit applications. Once a bus is instrumented with electronic guidance, it can provide lane assist along dedicated BRT lanes. In the applications where dedicated lanes are not available, lane assist can facilitate efficient operation at Queue Jump Lanes and can significantly benefit Bus Priority Systems. Electronic guidance can also support

application at a bus depot where BPD technology can be useful as a component of the concept of Advanced Maintenance Station.

PATH has demonstrated precision docking function on automobiles. The objective of the BPD project is to develop and enhance the precision docking system for real-world bus operations. At the project early stage, Caltrans and PATH have decided to develop and demonstrate automated BRT using three automated buses (Demo 2003). Because of the synergy of these two programs, and due to the safety critical nature of precision docking/lane assist functions, PATH and Caltrans have determined to focus this project to safety designs of precision docking system. The two projects will complement each other and the mutual goal is to accelerate the deployment of precision docking/lane assist technologies.

This final reports the fault analysis of precision docking system and safety design of the safety critical elements for precision docking system. The report includes three Parts, including:

Part I provides a description of the Precision Docking System and reports analysis for fault diagnosis and safety design of automated steering controller and Electronic Control Unit (ECU) for steering actuator. It also reports a demonstration PATH conducted during the National Intelligent Vehicle Initiative demonstration organized by the US Department of Transportation Joint Program Office.

Part II report an analysis and design for a reliable direct drive for the steering wheel column of buses.

Part III reports power system reliability.

The report below is the Part II report: A Reliable Direct Drive for the Steering Wheel Column of Buses. It evaluates the feasibility of using a direct drive for the steering wheel column of buses and heavy trucks. Permanent magnet technology is proposed for the motor design, due to its proven advantages for medium- to low-power servo applications. A redundant set of windings is introduced in the motor, together with a fault-detection/isolation system, to provide fault tolerance and increase the actuator's reliability. The report is organized as follows: first, the design of the motor is described. Next, the power electronics and control strategy are analyzed. Finally, fault-detection and fault-isolation techniques are presented.

2. System Design for Electronic Steering Actuator

The design of a direct drive actuation for the steering wheel in an automotive automatic steering application is considered here. The main goals of this design are: reliability and fault-tolerance, compact size and low weight, low cost, and adequate control performance.

The system proposed here consists of a permanent magnet (PM) motor whose rotor is attached to the steering wheel column (direct drive). The motor has 6 phases, arranged as two sets of 3-phase wye-connected windings. Each one of those sets is driven by an independent electronic inverter.

During normal operation, the 6 phases help to generate torque in a coordinated way. When a fault is detected, the faulty set is disconnected, and the entire load is transferred to the other 3-phase set.

Some fault-detection and fault-isolation mechanisms are discussed, pondering their advantages and disadvantages.

In Fig. 1, we show a diagram of the system.

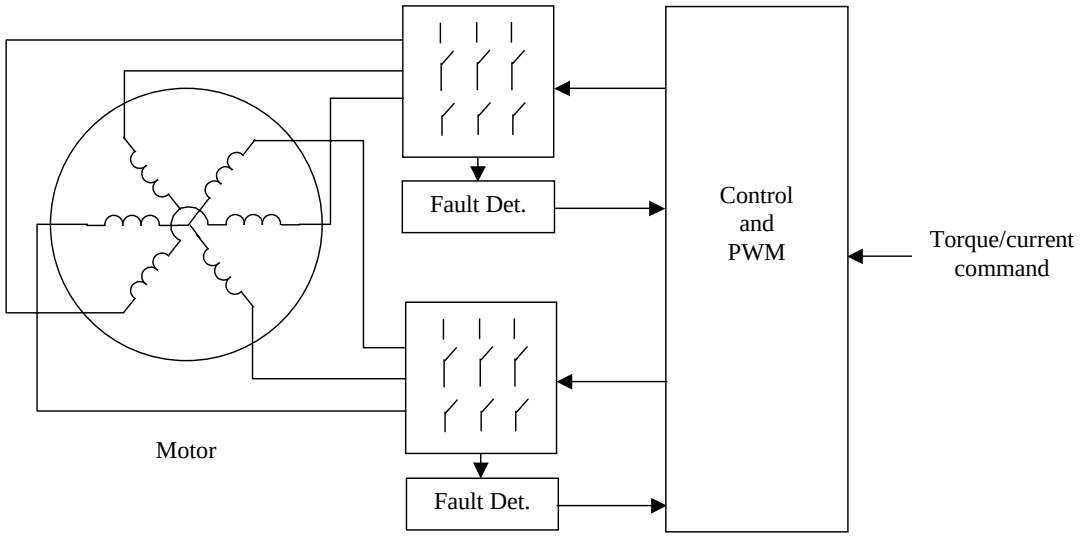

Figure 1- System diagram

.

2.1 Machine Design

A combination of developments in magnetic materials, electronic devices, and digital control systems, has recently generated an expansion in the use of permanent magnet brushless motors in servo applications. Brushless motors achieve higher torque-to-weight/size and torque-to-inertia ratios, than the traditional DC commutator motors. In addition, the absence of brushes implies higher reliability and less maintenance.

There are two types of permanent magnet brushless motors, depending on the back-emf waveform shape. Those with a trapezoidal shape are called brushless DC motors (BLDC), which are simple to control but may have significant pulsating torque. Those with a sinusoidal shape are called permanent magnet synchronous motors (PMSM), and can achieve very smooth torque at the expense of a more complex control.

Several methods have been developed to reduce the pulsating torque in BLDC motors, ranging from motor design to control techniques [4]. However, pulsating torque in the

steering wheel column is such a sensitive factor, that the industry choice for electric power-assisted steering is PMSMs, even if the controller cost is higher [13].

In [3], the torque ripple was computed for a BLDC motor design very similar to the one presented in this report. The results show that the peak-to-peak torque ripple amplitude is about 6% of the DC torque, and the width of the regions with diminished torque is about 10°. The net effect of the pulsating torque on the overall performance of the system can only be assessed by experimentation. Thus, the decision has to be deferred to a later stage in the development.

The torque rating of the actuator currently used in the bus automated steering prototype is 15Nm. It was observed that the prototype is under actuated, especially at low-speed, high-torque regime. The control engineers estimate that they need the double of that value. Therefore, we will design the actuator for 30Nm.

In the Appendix, we described the detailed design of a BLDC motor for this rating. The resulting dimensions are:

- machine length = 22 cm
- rotor diameter = 12 cm
- stator diameter = 14 cm

2.2 Control

As mentioned above, the control strategy depends on the type of motor being used. We assume that the control reference is a desired current, which is equivalent to a desired torque.

In the case of the BLDC, the control is very simple because we can use a six-step PWM strategy, regulating the phase currents to a constant value during each step. The strategy is illustrated in Fig. 2. The back-emf waveform has to be flat for 120°, as is usually the case in a carefully designed machine. In every 60° interval (called a step), the two phases that have a flat back-emf are fed with a constant current, while the phase whose back-emf

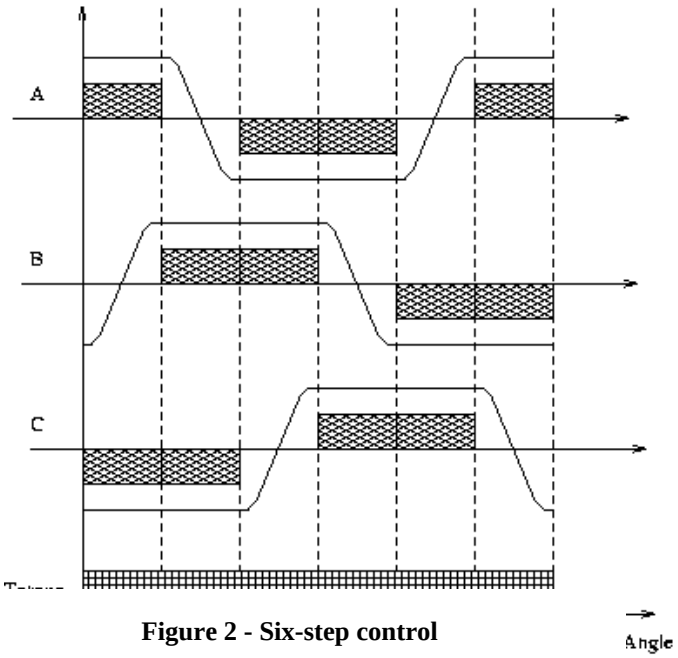

Figure 2 - Six-step control

is changing has no current. The torque, which can be expressed as $T=(e_A i_A+e_B i_B+e_C i_C)/\omega$, is ideally constant. Current regulation can be achieved using a single current sensor in the dc link [8].

In the case of the PMSM, a transformation between the fixed and rotating reference frames is needed, because torque is produced by the current component that is aligned with the magnetic field. The PWM strategy has to act on all phases to provide the desired current with the desired alignment.

In a wye-connected 3-phase system with isolated neutral, the currents are not independent and live in a two-dimensional space, called the α-β plane. In this plane, the orientation of the rotor field can be represented by a vector, which rotates as the rotor does. This defines a moving reference frame, called the d-q axes. Torque is generated by the component of the current that is aligned with the q-axis. Therefore, the controller has to provide the amplitude of currents on the three phases, such that the resultant in the α-β plane is aligned with the q-axis. Precision rotor position information is needed in order to perform vector control in the d-q axis; this is usually a drawback for PMSMs, but in our case that information is already available as part of the outer control loop for the steering angle.

3. Fault-tolerance

We identify first, the potential faults that can occur. These are [7]:

- phase winding short circuit at the terminals
- switch open circuit
- switch short circuit

Notice that we are explicitly excluding a fault in the rotor position sensor, which is a critical part of the system. The reason for this exclusion is that the solution to this fault scenario would be either to add one or two more position sensors, or include a sensorless control algorithm [6]. As mentioned before, the rotor position sensor is already part of an outer control loop, so reliability issues should be addressed at that level.

We also want to mention that, as justified in [9], the faults generated inside the machine (e.g., winding insulation failure) are very unlikely to occur, and are not considered. Similarly, the simultaneous occurrence of multiple faults is very remote.

The strategy will be to detect and isolate the faulty phase or group of phases, transferring the entire load to the remaining phases. Therefore, fault-tolerance is achieved by the following components: redundant actuators, fault detection, and fault isolation.

3.1 Redundant Actuators

In our design, there are two independent 3-phase windings with their corresponding inverters, offering the desired redundancy. They can work together as a 6-phase system, but in case of a fault, one of them can carry the total load.

This is not the only way of achieving redundancy. We can think of a system with n+1 phases, where each phase winding is independent and driven by a full H bridge. In this case, if one of the phases has a fault, the rest can continue to operate. We will present an example of a system like that and compare it with the one proposed above.

It is enough to have two phases in order to generate torque, however this has the disadvantage that, in some rotor position, the net torque produced is zero, therefore leading to potential startup problems. Consequently, we look for $n \geq 3$. The first option, $n=3$, implies that the system would have 4 phases during normal operation; since 4 phases have a torque ripple performance like 2 phases, we discard this option. The next one, is $n=4$, which implies that during normal operation the system will have 5 phases. This is an attractive option, and we study it further.

A 5-phase system would require one H bridge per phase, therefore 20 switches, and one current sensor per phase, therefore 5 current sensors. On the other hand, a 6-phase system arranged as two 3-phase systems, would require two 3-phase inverters, therefore 12 switches, and one current sensor per 3-phase system, therefore only 2 current sensors.

The cost advantages of the 6-phase system are evident. However, the torque ripple performance of the 5-phase system should be better than that of the 6-phase system, because the latter has the same performance as a 3-phase system.

Hence, the choice of the number of phases depends on the trade-off between the torque ripple performance and the cost.

The above reasoning is valid both for PMSM and for BLDC motors. However, in the case of the PMSM, the 5-phase system requires a more careful analysis of the vector control strategy.

We conclude that the chosen number of phases is a good fault-tolerant compromise between cost and torque ripple.

3.2 Fault Detection

As suggested by [5], fault detection in power devices can be simply achieved by comparing the voltages at the device outputs and checking if they correctly follow the corresponding triggering signals. This method, though, requires a precise tuning and synchronization.

Other more complex systems are possible. In [11], a model-based fault detection system for BLDC is described. This system uses a reduced number of sensors, namely a bridge supply current sensor, a bridge voltage supply sensor, and a rotor angular speed sensor. However, faults are difficult to individualize, and there are issues in guaranteeing the persisting excitation that is needed for the parameter estimation.

In [10], an expert system is used to detect and identify faults in AC drives. Although the focus of the paper is on off-line diagnosis, the same approach can be applied for on-line system monitoring. The number of sensors needed for this is very high, though.

A comprehensive analysis of detection techniques is described in [12]. The cost/benefit ratio of different techniques is addressed for the case of an open switch fault. Similar results can be derived for other types of faults.

3.3 Fault Isolation

The faulty phase or group of phases can be isolated by blowing conveniently located fuses [5]. The circuit is shown in Fig. 3, for one inverter pole. The phase is isolated by firing SCRA+ and SCRA-, creating a current that blows the fuses. Capacitors Ci block the DC path through the SCRs, allowing them to turn off.

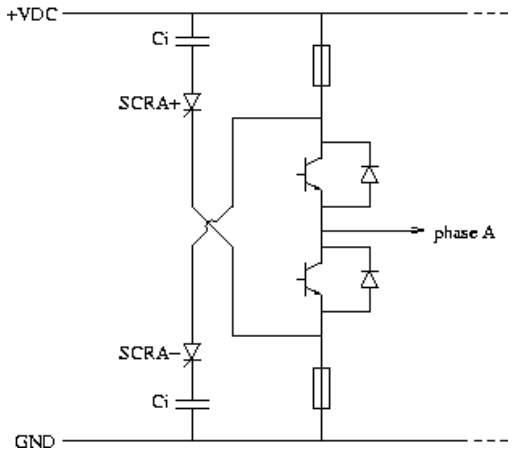

Figure 3 - Fault isolation circuit

Conclusions

The feasibility of using a reliable direct drive based on a permanent magnet motor for the steering wheel column was studied. A design solution was outlined, consisting of the following pieces:

- a six-phase BLDC motor, with two sets of wye-connected three-phase windings
- a pair of three-phase inverters, working together on the six phases during normal operation
- a six-step PWM strategy controlling each inverter
- a fault detection system
- a fault isolation system

In case a fault occurs, the complete three-phase sub-system (inverter plus windings) is isolated, and the remaining sub-system takes the entire load, working as a conventional three-phase motor.

The solution described in this report needs to be validated in an experimental prototype. The main issue to be addressed is the torque ripple generated by the BLDC motor. It

should be assessed if this is acceptable or not for the application. In case it is not, a PMSM should be used, with the consequent changes in the design of the motor and the control strategy.

Appendix: BLDC Motor Design

We use design equations extracted from [1] and [2].

1) Number of Poles and Phases

We propose a design similar to the one presented in [3]. The motor has 10 poles and 12 slots, with 6 phases arranged in two 3-phase sets, each one of them being wye-connected. This arrangement provides the desired redundancy, because each 3-phase set can handle the load in case the other one fails.

In Fig. 4, we show a cross-sectional view of the machine. The two 3-phase sets are distinguished by a subscript. The winding pitch is equal to one, giving a good utilization of copper, and, since there is no winding overlapping, the mutual inductance is low. The number of slots per pole is fractional, which reduces the cogging torque.

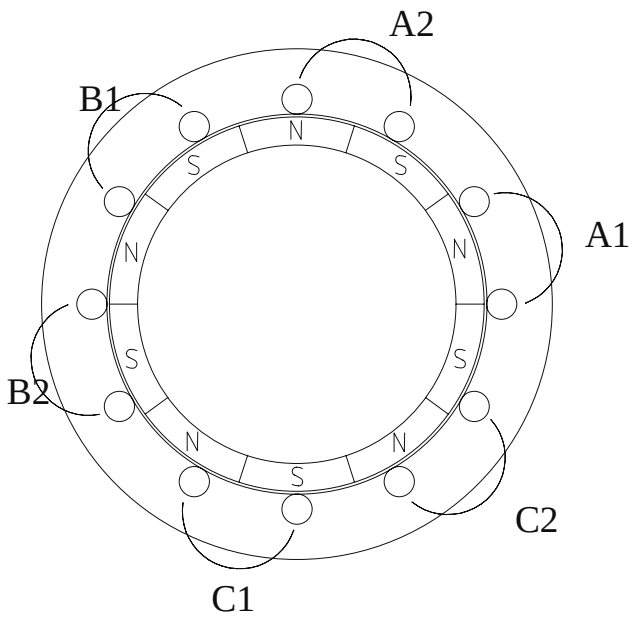

Figure 4 - Cross-sectional view of the BLDC motor

2) Magnetic design

We select an air gap g=0.75m and a permeance coefficient PC=10. Then the magnet length (in the radial direction) is L_M=10g=7.5mm. The magnetic material chosen is TDK-FB4B (a standard ferrite), which provides a flux density B_M=0.35T for this permeance coefficient at 40°C. There are better materials available at a higher cost, but are not considered in this initial design.

3) Rotor Design

The rotor size can be roughly estimated by the equation $T=kD_r^2L$, where T is the torque, D_r is the rotor diameter, L is the rotor length, and k is an empirical constant. For our type of motor, $k=1.4lbf.in/in^3=9.65x10^3N/m^2$ [1].

For a torque T=30Nm, we select a rotor diameter $D_r=0.12m$, and we have L=0.216m. The rotor yoke diameter, though, is $D_{ry}=D_r-2L_M=0.105m$.

The magnet length in the axial direction is augmented to overcome the overhang effect, therefore $L_r=L+L_M=0.2235m$.

This gives a magnet pole area $A_M=\pi D_{ry}L_r/P=7.37x10^{-3}m^2$. The flux per pole is then $\Phi=B_MA_M=2.58x10^{-3}Wb$.

4) Estimation of k_E,k_T

We can roughly estimate the value of the back-emf constant for this machine by imposing that the back-emf voltage generated at maximum speed should be close to the DC bus voltage. We estimate the maximum speed as 2 turns per second, i.e., 4π rad/s. Then, $k_E=24V/4\pi rad/s=1.91Vs/rad$. The torque constant has the same numerical value: $k_T=1.91Nm/A$.

5) Number of Turns

The number of conductors needed to generate the back-emf constant computed above in a 3-phase system, for the magnetic flux available, is given by the equation $Z=3/2\ k_Ea\pi/\Phi CP$, where a=1 and $C\approx0.9$. Then Z=349. Since we have 6 slots per 3-phase system, then the number of turns per coil (which is the same as the number of conductors per slot) is z=349/6}=58.

6) Stator Dimensions

In this section, we compute the dimensions of the stator laminations, illustrated in Fig. 5.

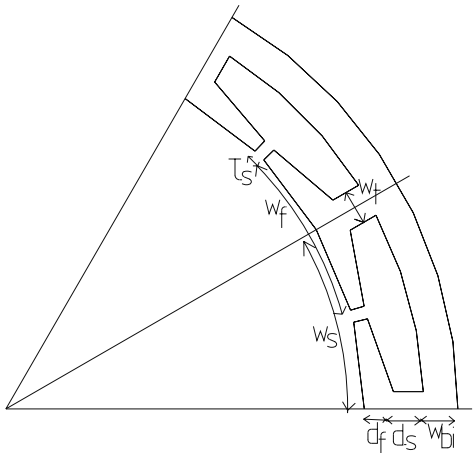

Figure 5 - Stator dimensions

The width of the teeth has to carry the flux without saturation, then $w_t=0.9x10/12x\Phi/B_{sat}L=3.5mm$ (for $B_{sat}=1.5T$). The slot pitch at the airgap is $w_s=(D_r/2+g)x2\pi/12=31.8mm$. Given a feet separation of $\tau_s=1mm$, the foot width is $w_f=w_s-\tau_s=30.8mm$. The back-iron width is $w_{bi}=0.9\Phi/2B_{sat}L=2.1mm$.

The slot current can be computed from the torque using the Blv formula: $I_s=T/B_gLxD_r/2x12=551A$. The slot area has to accommodate this current, then $A_s=I_s/J_{max}k_p$, where $J_{max}=500A/cm^2$ is the maximum current density in the copper without a cooling system, and $k_p=0.6$ is the packing factor. Then, $A_s=1.84cm^2$. By selecting $d_f=2mm$, this gives us the radial length of the slot, which has to be $d_s=5.9mm$.

Finally, the stator outer diameter is $D_s=D_r+2(g+d_f+d_s+w_{bi})=0.141m$.

7) Electrical Parameters

The mean length of a turn can be estimated as $MLT=2L+2x2\pi/12(D_r/2+g+d_f+d_s/2)+4x1mm=0.525m$. The wire diameter is $D_w=\sqrt{(A_sk_p/z)}=1.4mm$. We select a wire type AWG14, whose resistivity is $\rho=8.5m\Omega/m$. Then the coil resistance is $R=\rho MTLz=0.26\Omega$.

The copper losses at maximum torque are $P_{Cu}=2R(I_s/z)^2=47W$ (there are only two phases active at the same time), but during normal operation the current is much lower and so is the lost power. Other losses, like core losses, are not significant due to the low frequency of operation.

Bibliography

[1] J.R. Hendershot Jr. and T.J.E. Miller. Design of Brushless Permanent-Magnet Motors. Magna Physics, 1994.

[2] D.C. Hanselman. Brushless Permanent-Magnet Motor Design. McGraw-Hill, 1994.

[3] T. Izhar and P.D. Evans. Permanent Magnet Multipole 6-phase Brushless DC Motor for Automotive Applications. Proceedings of the European Power Electronics Conference, 1997.

[4] T.M. Jahns and W.L. Soong. Pulsating Torque Minimization Techniques for Permanent Magnet AC Motor Drives---A Review. IEEE Transactions on Industrial Electronics, Vol. 43, No. 2, April 1996.

[5] S. Bolognani, M. Zigliotto, and M. Zordan. Experimental Fault-tolerant Control of a PMSM Drive. Proceedings of the IEEE Conference on Industrial Electronics, 1998.

[6] S. Green, D.J. Atkinson, A.G. Jack, B.B. Mecrow, and A. King. Sensorless Operation of a Fault-tolerant PM Drive. IEE Proc. on Electr. Power Appl., Vol. 150, No. 2, March 2003.

[7] B.C. Mecrow, A.G. Jack, J.A. Haylock, and J. Coles. Fault-tolerant Permanent Magnet Machine Drives. IEE Proc. on Electr. Power Appl., Vol. 143, No. 6, November 1996.

[8] T.M. Jahns. Motion Control with Permanent-Magnet AC Machines. Proceedings of the IEEE, Vol. 82, No. 8, August 1994.

[9] D. Kastha and B.K. Bose. Investigation of Fault Modes of Voltage-Fed Inverter System for Induction Motor Drive. Proc. of the IEEE Industry Applications Society Annual Meeting, 1992.

[10] K. Debebe, V. Rajagopalan, and T.S. Sankar. Diagnosis and Monitoring for AC Drives. Proc. of the IEEE Industry Applications Society Annual Meeting, 1992.

[11] O. Moseler and R. Isermann. Application of Model-Based Fault Detection to a Brushless DC Motor. IEEE Trans. on Industrial Electronics}, Vol. 47, No. 5, October 2000.

[12] R.L. de Araujo Ribeiro, C.B. Jacobina, E.R. Cabral da Silva, and A.M. Nogueira Lima. Fault Detection of Open-Switch Damage in Voltage-Fed PWM Motor Drive Systems. IEEE Trans. on Power Electronics}, Vol. 18, No. 2, March 2003.

[13] A.W. Burton. Innovation Drivers for Electric Power-Assisted Steering. IEEE Control Systems Magazine, Vol. 23, No. 6, December 2003.

Electronic Control Unit Modelling and Health monitoring:

The electronic control unit (ECU) is current driver regulator. In this chapter, a dynamic model for the ECU of the assist torque motor will be devoloped with a fault estimation and monitoring identify faults that could occur due to gain changes in the ECU.

ECU Modelling:

The ECU is a current amplifer empowerd with a CPU (micro-controller device) to perform such functions as estimating the friction and load torque acting on the motor to compensate for their presence. The ECU also monitors the current input to the motor ensuring that it lies below the limiting value. The NSK ECU block diagram structure is given as follows:

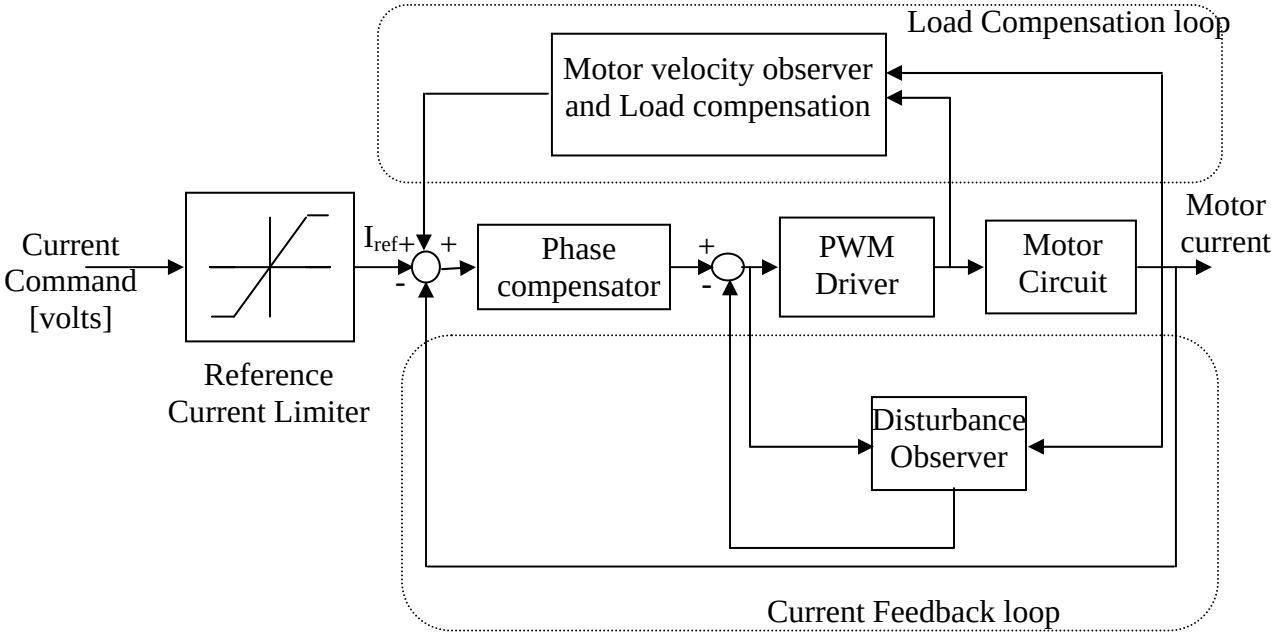

Figure 1: ECU functional block diagram

From above block diagram, the following components carry out the essential functionality of the ECU block:

- Reference current limiter: limits the values of the reference current to ± 25 Amps;

- Phase compensator: regulates the error between the reference current and the feedback current to zero;
- PWM Driver: generates the driving motor voltage, for the NSK ECU the PWM is driven at 20 KHz. In the following analysis the PWM dirver will be ignored;
- Motor circuit: models the dynamics of the DC motor attached to the ECU block;
- Motor velocity observer and load compensator: estimates the motor velocity and approximates the load inertia (which includes the load torque T_l) and back emf to compensate for them in the reference current;
- Disturbance Observer (DOB): estimates the load torque acting on the DC motor and compensates for it.

The following analysis will focus on the current feedback loop to obtain its dynamical model for current regulation and FDI development.

Current Loop:

In DC motors, the current loop is the control unit for both position and velocity regulation. The ECU block diagram presented in fig. 1 is made up of 2 loops the current feedback loop and the load torque compensation loop. The current feedback loop and the motor circuit are expanded into the following block diagram:

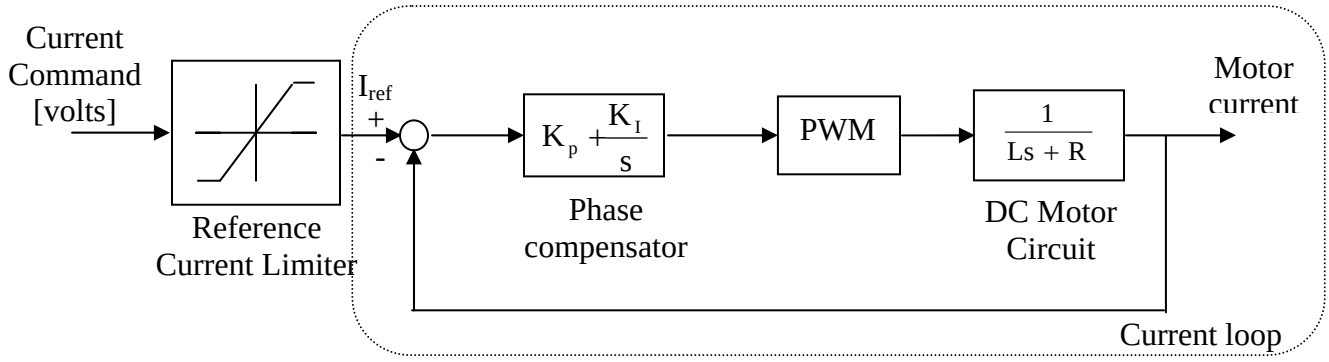

Figure 2: ECU DC motor current feedback loop block diagram

Based on the above block diagram, the input-ouput model of the ECU current loop (dashed box) is derived by conducting system identification experiments. The input is the current command voltage signal and the output is the motor current. The motor current is measured using an external current sensor which measures the equivalent

current in volts. The measured motor current is then connected to the computer data acquisition system.

Identification Experiments:

System identification experiments were conducted to identify the input-output transfer function for the ECU current driver. The following setup was used:

- Perturbation signal: 16 bit register PRBS (pseudo random binary sequence);
- Sampling period $\Delta t = 0.01$ sec;

Using the *System Identification Toolbox* in Matlab, the following plot shows the input signal and the output current (in volts) of the ECU:

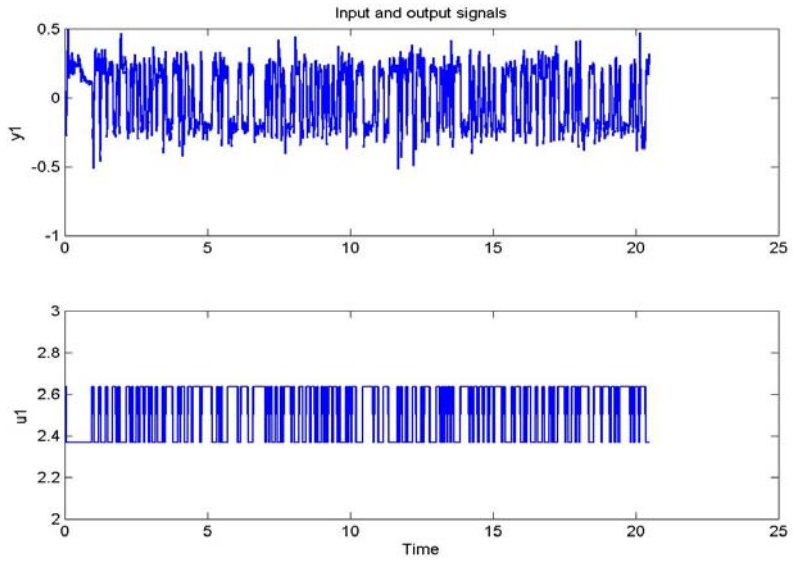

Figure 3: ECU identification: sampled response (top) and RRBS signal (bottom)

Using an output error model whose general structure is given by:

$$y(t) = \frac{B(z)}{F(z)}u(t-k) + e(t)$$

where, the parameters in the model are:

- y is the output,
- u is the input,
- t is the sampled time instant,
- k is the delay in the model,
- e is the output error,

A second order model is fitted to the input-output data with a delay parameter k = 1. The following parameters are identified (the B(z) polynomial includes the delay):

$$F(z) = 1 - 1.5256z^{-1} + 0.5256z^{-2} \qquad B(z) = -0.8296z^{-1} + 0.8296z^{-2}$$

Model Validation Results:

Several PRBS as well as sweeping sine signals are applied to the ECU current reference input and the sampled output current results (in volts) are used to validated the ECU model as given above. The model validation results are shown below:

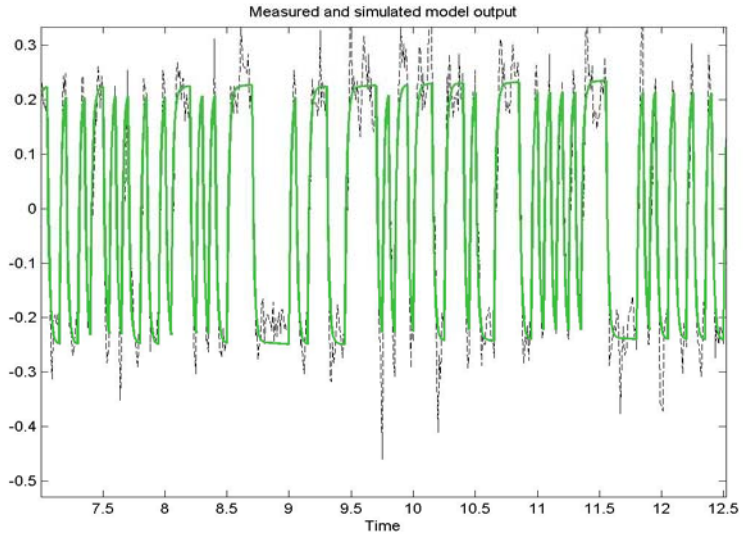

Figure 4: ECU model validation: sampled PRBS response (dashed) and model output (solid)

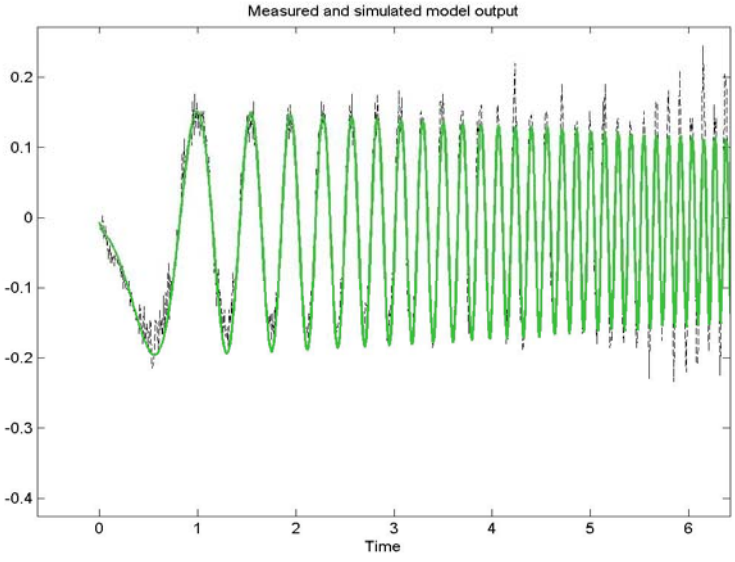

Figure 5: ECU model validation: sampled sweep-sine response (dashed) and model output (solid)

The ECU model is converted to the continuous time domain and the following transfer function is obtained:

$$\frac{Y(s)}{U(s)} = \frac{-112.5s + 0.05067}{s(s + 64.34)} \text{ [volts/volts]}$$

Ignoring the fast right-half plane zero (introduced by sampling), the ECU transfer function is simplified to:

$$\frac{Y(s)}{U(s)} = \frac{-112.5}{s + 64.34} \text{ [volts/volts]}$$

It is noted that the negative sign in the above transfer function is due the polrity reversal of the current sensor.

Fault Monitroing and Estimation of the ECU (FDI):

The ECU is equipped with internal diagnostic functions that are mainly concerned with abnormal changes in the current reference signal and the battery voltage signal level. Other diagnostic fuctions monitor the motor condition (i.e. whether the motor is on or off) and its temperature. The ECU documentation tabulates the detection conditions for possible faults and the associated recovery condition. The purpose of this section is to design a fault estimation filter that detects faults due to changes in the internal dynamics of the ECU motor current loop. In particular, the focus will be on the variation in the gain of the ECU current loop. For this purpose, an external potentiometer is connected to the current command input signal such that varying the potentiometer position (introducing external resistance) will simulate the effect of a gain drop in the ECU unit. The overall all ECU unit with the potentiometer and the current sensor are shown below:

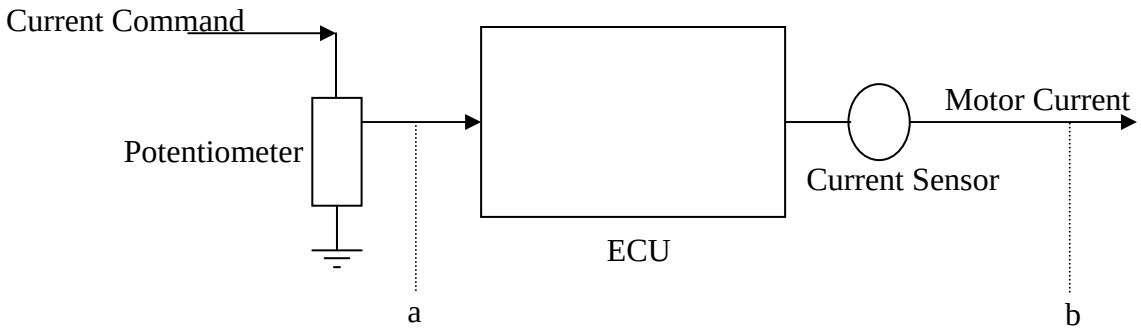

Figure 6: Fault detection setup for the ECU unit

In the figure above, measurements are made at the two points denoted as *a* and *b*. Where at point *a* the current command influenced by the potentiometer is sampled to the data acquisition system and at point *b* the resulting motor current measurement is also sampled to the data acquisition system.

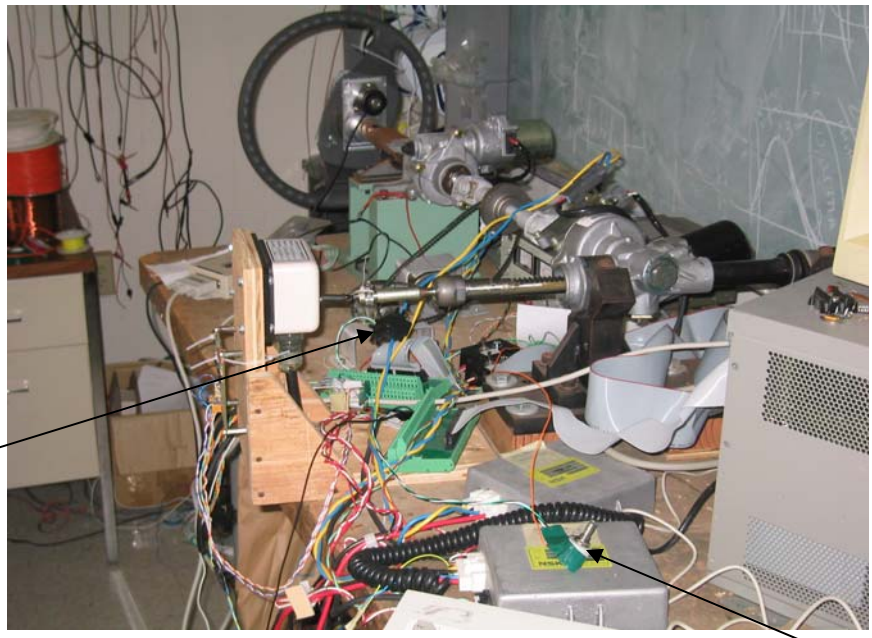

Figure 7: Fault detection setup for the ECU unit

The concept of fault monitoring is basically the design of a filter (known as "residual" generator) to estimate (and hence detect) the value of a given fault. Various approaches have been developed in the time and frequency domains for the design of residual generators. The most straight forward methods rely on using obsevers or models of the plant for which the FDI is investigated. A fundamental design criterion for residual generators is the minimize the effects of any disturbance or noise acting on the plant on the residual output. For the ECU transfer function model above, a model based residual generator is presented in the diagram below:

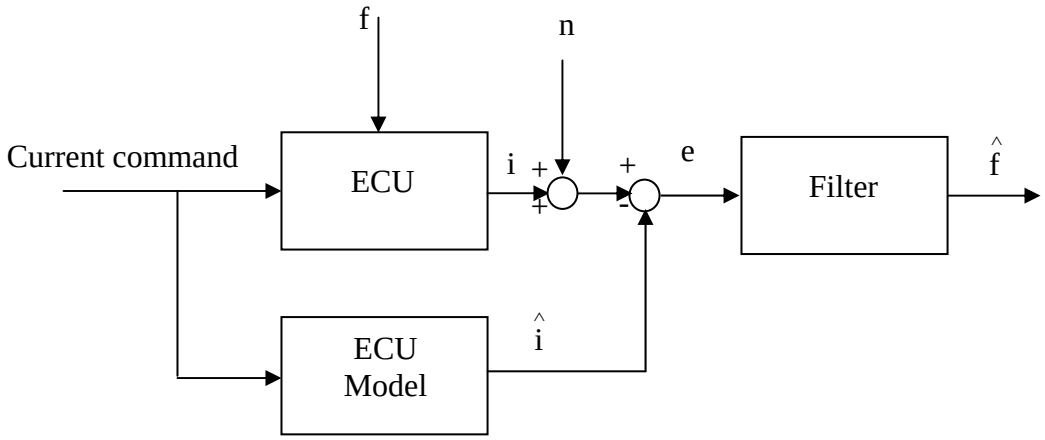

Figure 8: ECU model based FDI filtering

In the figure above, the following parameters are defined below:

Parameter name	Definition
f	Additive fault due to the potentiometer influence on the ECU gain
i	Output current
n	Measurement noise due to current sensor
$\hat{i}$	Output current of the ECU model
e	Difference between actual current measurement and current given by the ECU transfer function model
$\hat{f}$	Estimate of the actual fault

Table 1: Model based FDI parameters for the ECU

Filter Design for the Fault Monitoring:

It is clear from figure 7 above, that the fault monitoring problem is based on the design of a filter to produce the estimate of the fault given by $\hat{f}$. For this purpose, let F denotes the designed filter and u denotes the current command, then using standard H_∞ optimization methods, the following cost function is minimized by designing the (sub) optimal filter F_{opt} in the H_∞ sense:

$$J = \min_{F} \frac{\left\| f - \hat{f} \right\|_2}{\left\| u \right\|_2}$$

Using the *Mu Analysis and Synthesis Toolbox* in Matlab, the following H_∞ optimal filter is designed:

$$F(s) = \frac{\hat{f}(s)}{e(s)} = -\frac{212.4s^2 + 1.897e4s + 3.416e5}{s^3 + 539.8s^2 + 3.603e4s + 5.77e5}$$

For implementation, the above filter transfer function is discretized with sampling period of 0.01 sec.

Experimential Results:

Several experiments were conducted to assess the filtering performance of the desinged FDI filter. Using the potentiometer, a fault of magnitude -0.4 volts in the form of a pulse (of finite duration) is imposed on the ECU. The following plot is then obtained:

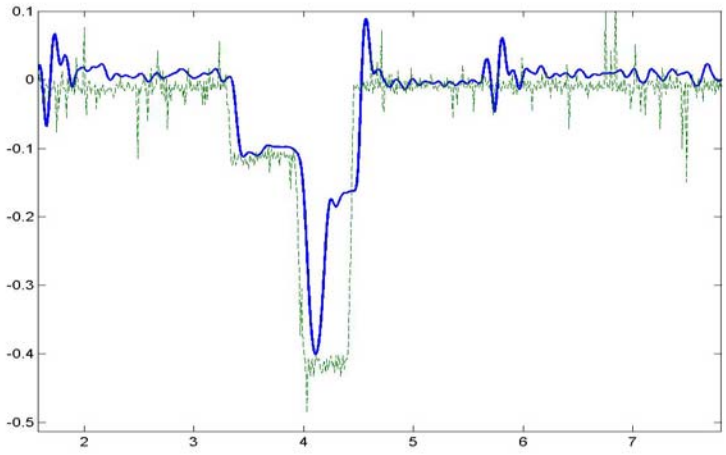

Figure 9: Single fault, FDI filtering (solid) and experimental result (dashed)

Using the potentiometer, three faults of magnitudes -0.74, -0.2, -0.17 and –0.1. volts in the form of finite duration pulses are imposed on the ECU as the following plot shows:

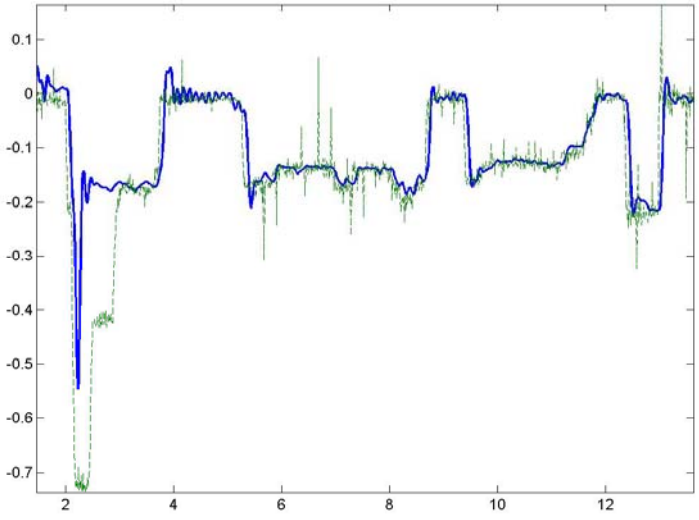

Figure 10: Multiple faults, FDI filtering (solid) and experimental result (dashed)